Electrochimica Acta xxx (2012) xxx–xxx

Contents lists available at SciVerse ScienceDirect

Electrochimica Acta

journal homepage: www.elsevier.com/locate/electacta

Effect of overcharge on entropy and enthalpy of lithium-ion batteries

Kenza Maher [a,*], Rachid Yazami [a,b]

[a] Nanyang Technological University, Energy Research Institute @ NTU (ERI@N), Research Techno Plaza, X-Frontier Blk, 50 Nanyang drive, Singapore 637553, Singapore
[b] Tum Create, 1 Create Way, #10-02 Create Tower, Singapore 138602, Singapore

ARTICLE INFO

Article history:
Received 20 July 2012
Received in revised form 9 November 2012
Accepted 10 November 2012
Available online xxx

Keywords:
Thermodynamics
Entropy
Enthalpy
High voltage charge
Lithium-ion batteries

ABSTRACT

We have investigated the evolution of the thermodynamics behaviour and of the crystal structure of electrodes materials of lithium-ion batteries based on graphite anode and lithium cobalt oxide (LCO) cathode after applying high voltage charging between 4.2 V and 4.9 V cut-off voltages (COV). We found the entropy and enthalpy profiles vary dramatically with the applied COV. These changes correlate well with the anode and the cathode crystal structure degradation as evidenced by post-mortem X-ray diffractometry and Raman scattering spectrometry.

Our finding is thermodynamics measurements can be used as a new and non-destructive investigation tool to characterize the degradation level of electrode materials and consequently assess the cell's state of health (SOH).

1. Introduction

In recent years we have developed electrochemical thermodynamics measurements (ETMs) methods and tools, which we applied to lithium battery half-cells to analyse anode [1–3] and cathode [4] materials. The method consists of monitoring the evolution of the cell' open-circuit voltage (OCV), 'E_0', with the cell temperature, 'T', at different states of charge (SOC). The later correspond to the lithium stoichiometry in the anode and the cathode, 'x', in Li_xC_6 and $Li_{1-x}CoO_2$, respectively. The entropy $\Delta S(x)$ and enthalpy $\Delta H(x)$ state functions can be computed from the general thermodynamics laws:

$$\Delta S(x) = F\frac{\partial E_0(x)}{\partial T} \quad (1)$$

$$\Delta H(x) = -F\left(E_0 + T\frac{\partial E_0(x)}{\partial T}\right) \quad (2)$$

Since $\Delta S(x)$ and $\Delta H(x)$ in Eqs. (1) and (2) are measured at a defined state of charge of the battery, 'x', $\Delta S(x)$ and $\Delta H(x)$ can be defined as the local slope of the battery system' total entropy and the total enthalpy variation vs. 'x', respectively. Accordingly, there is no need for a reference state to determine $\Delta S(x)$ and $\Delta H(x)$ [5].

In this work full lithium-ion batteries (coin cells 2032) were subjected to overcharge between 4.3 V and 4.9 V COV, a process known to accelerate the cell's storage performances resulting from electrodes and electrolyte materials degradation [6,7].

We followed the cells ageing and the changes in the $\Delta S(x)$ and $\Delta H(x)$ profiles as function of the COV. Results show important changes took place in the cell's thermodynamics behaviour which correlates well with increased anode and cathode materials degradation with COV. These results were supported by post-mortem X-ray diffraction (XRD) and Raman spectrometry analyses.

2. Experimental

Lithium-ion coin cells (LIR 2032) rated ~44 mAh were subjected to the following test steps:

2.1. High voltage ageing

A first set of cells were cycled with an Arbin Instruments battery cycler at the ambient temperatures in two steps:

(i) discharge at C/4-rate to 2.75 V and,
(ii) charge to a set COV at C/4-rate. For each test cell the COV was incremented by 100 mV from 4.2 V to 4.9 V. Once the COV reached, the cell is set to rest.

This first set of test cells will be designed hereafter "COV1".

The second set of cells were subjected to steps (i) and (ii), except at the end of step (ii) constant COV was maintained for 1 h for further cells ageing. This second set of cells will be denoted "COV2".

* Corresponding author. Tel.: +65 96627561; fax: +65 63163195.
E-mail addresses: Kenza.maher@tum-create.edu.sg (K. Maher), rachid@ntu.edu.sg (R. Yazami).

0013-4686/$ – see front matter © 2012 Elsevier Ltd. All rights reserved.
http://dx.doi.org/10.1016/j.electacta.2012.11.057

Table 1
LIB cells charge and discharge data vs. COV where q_{C2}, q_{D3}, q_{D4} refer to charge (C) and discharge (D) capacity during steps (ii), (iii) and (iv), respectively, $\langle e_{C2}\rangle$ and $\langle e_{D4}\rangle$ refer to the average charge and discharge voltage at steps (ii) and (iv), respectively, and q_{CL} refer to the discharge capacity loss between step (i) and step (iv).

COV (V)	q_{C2} (mAh)	$\langle e_{C2}\rangle$ (V)	q_{D3} (mAh)	q_{D4} (mAh)	$\langle e_{D4}\rangle$ (V)	q_{CL} (%)
4.2	43.91	3.88	43.60	43.07	3.82	0
4.3	46.67	3.93	45.47	42.51	3.81	1.30
4.4	49.37	3.97	47.54	41.44	3.80	3.78
4.5	53.13	4.01	50.43	40.62	3.78	5.69
4.6	64.44	4.11	59.94	38.09	3.77	11.56
4.7	72.99	4.17	65.71	37.35	3.76	13.28
4.8	72.78	4.20	64.35	36.16	3.77	16.04
4.9	72.53	4.28	63.86	34.90	3.62	18.97

In step (iii) cells of COV1 and COV2 sets were further discharged to 2.75 V at C/4 rate. Then in step (iv) the cells were charged to 4.2 V and re-discharged to 2.75 V at the same C/4 rate.

The charge (C) and discharge (D) capacities achieved in steps (ii), (iii) and (iv) are hereafter designed q_{C2}, q_{D3} and q_{D4}, respectively.

2.2. Thermodynamics measurements

Discharged cells after step (iv) were transferred to the Electrochemical Thermodynamics Measurements System (ETMS, BA-1000®, KVI Pte Ltd., Singapore). Cells undergo a "conditioning" cycle in which they are charged to 4.2 V and discharged to 2.75 V to determine their actual capacity. Then the cells are charged step-by-step up to 4.2 V. At each increment the SOC was increased by 5% by applying a constant current (~6 mA) for an appropriate duration time (~20 min). The actual current and time are fixed by the ETMS according to the number of data points set by the user and the cell rated capacity determined in the conditioning step. In our experiments we fixed the number of data points to 21; thus covering the full range of SOC from 0 to 100% by 5% increments.

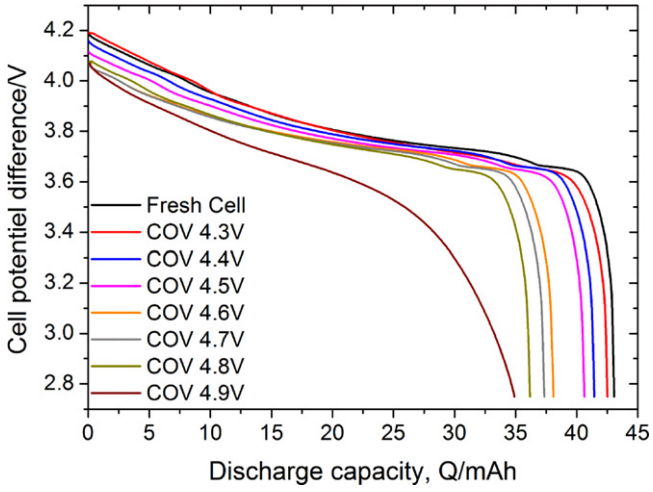

Fig. 1. Discharge profiles of LIB cells subjected to different charge cut-off voltages (COV).

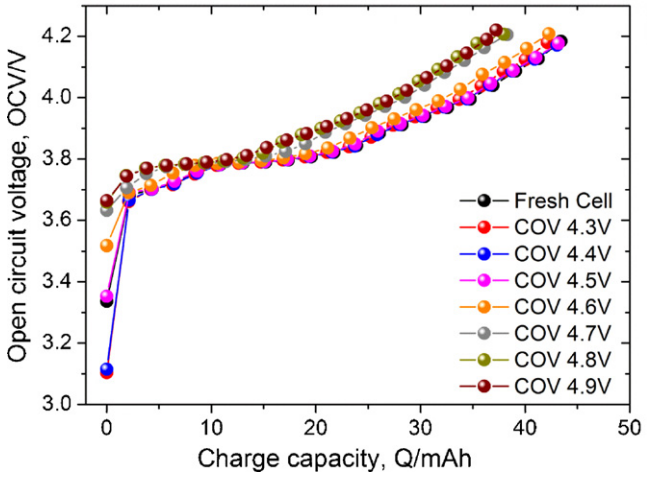

Fig. 2. OCV profiles of LIB cells versus the charge capacity during charge. Cells were subjected to different COV.

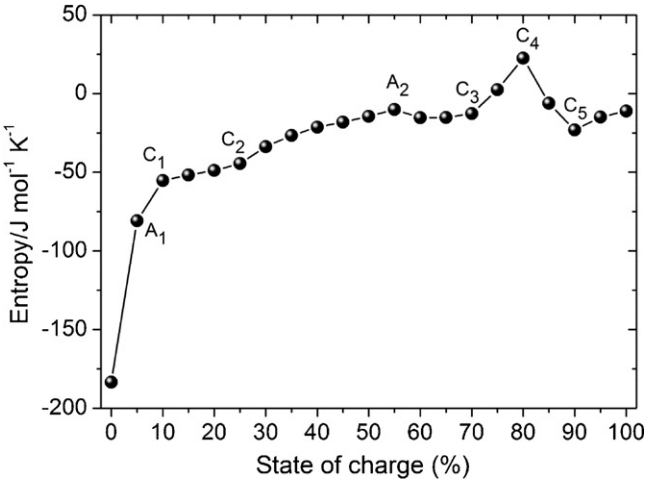

Fig. 3. Entropy profile vs. SOC of a fresh cell during 1st charge. The A_i and C_i points correspond to phase transitions in the graphite anode and the lithium cobalt oxide cathode, respectively.

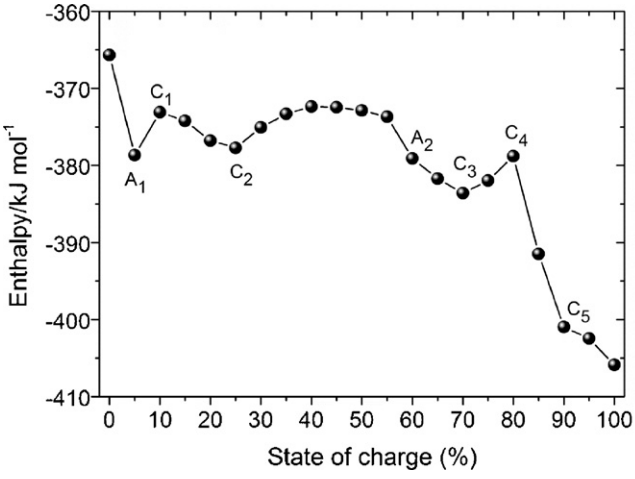

Fig. 4. Enthalpy profile vs. SOC of a fresh cell during 1st charge. The A_i and C_i points correspond to phase transitions in the graphite anode and the lithium cobalt oxide cathode, respectively.

Please cite this article in press as: K. Maher, R. Yazami, Effect of overcharge on entropy and enthalpy of lithium-ion batteries, Electrochim. Acta (2012), http://dx.doi.org/10.1016/j.electacta.2012.11.057

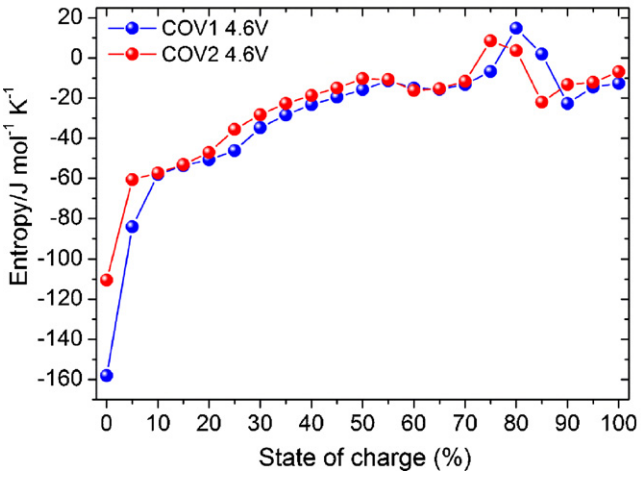

Fig. 5. Comparison of entropy profiles of COV1 and COV2 tests at 4.6 V.

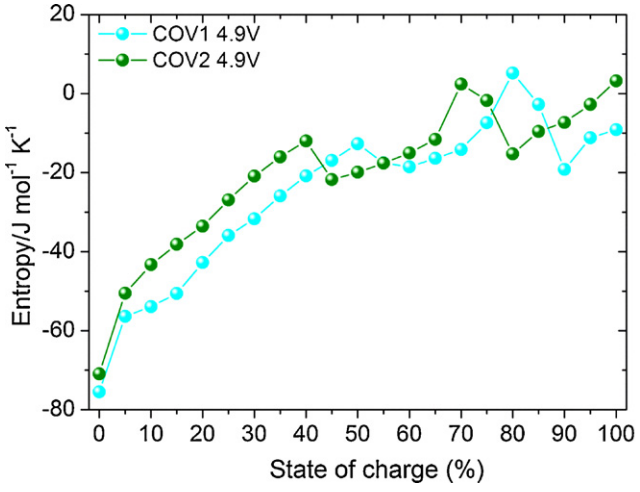

Fig. 6. Comparison of entropy profiles of COV1 and COV2 tests at 4.9 V.

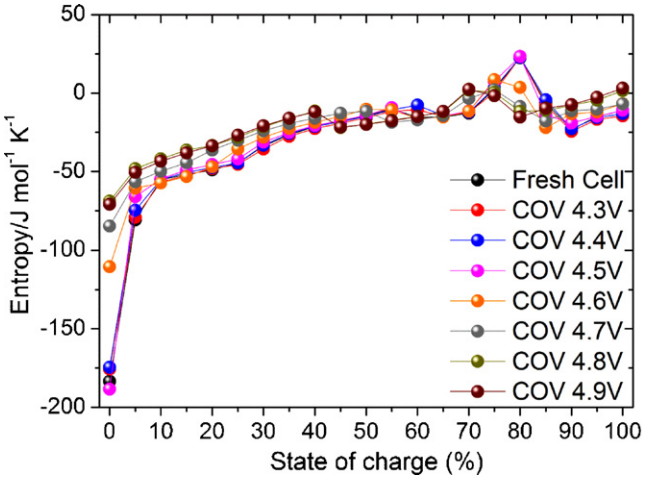

Fig. 7. Entropy profiles at different charge cut-off voltages.

At each SOC, the cell temperature T was automatically cooled from the ambient temperature of about 25–10 °C by ~5 °C increments while the OCV was monitored until it stabilized at a set T. The BA-1000 instrument converts $E_0(x,T)$ data to $\Delta S(x)$ and $\Delta H(x)$ data according to Eqs. (1) and (2), respectively.

In all COV1 and COV2 tests two test cells were used to check for reproducibility.

At the end of the ETM tests described above cells were discharged to 2.75 V. Selected cells at their discharge state were open in a glove box filled with argon; the anode and the cathode were retrieved and washed with DMC then they were dried in argon and in vacuum at the ambient temperatures. Electrode materials were then analysed by XRD on a Bruker D8 Advance diffractometre using Cu Kα radiation in the angular range of 15–90° (2θ) for cathode and 20–90° (2θ) for anode with a 0.02° (2θ) step, and by Raman scattering spectrometry, using Renishwa inVia Raman microscope in

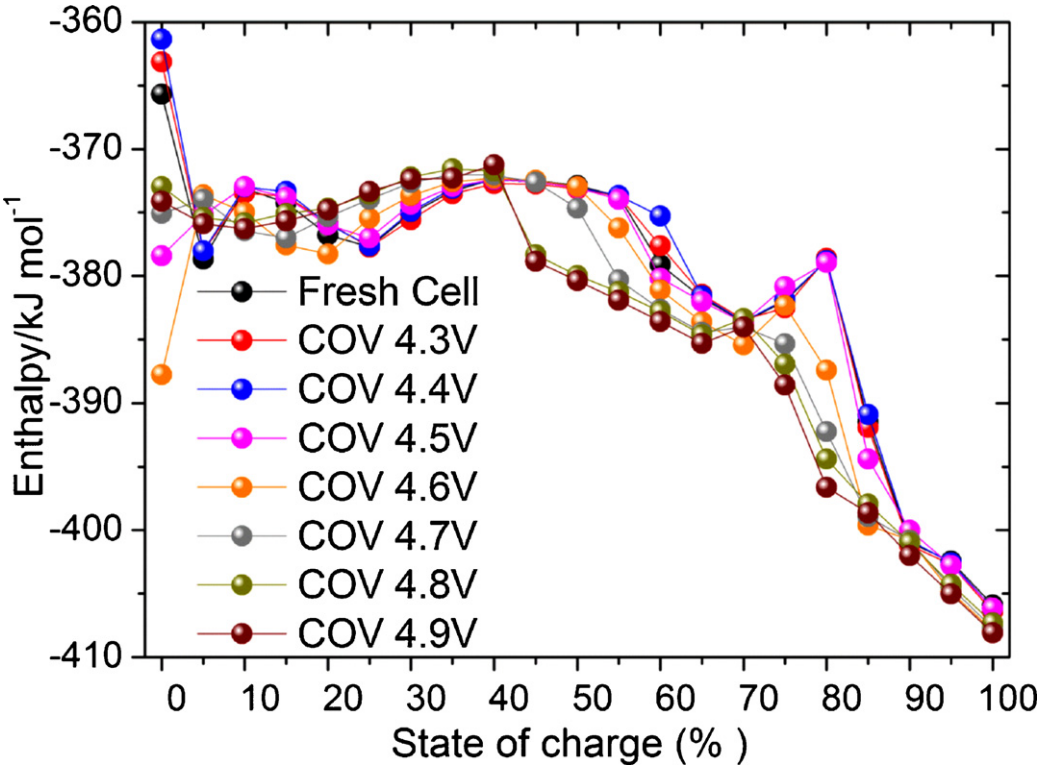

Fig. 8. Enthalpy profiles at different charge cut-off voltages.

Please cite this article in press as: K. Maher, R. Yazami, Effect of overcharge on entropy and enthalpy of lithium-ion batteries, Electrochim. Acta (2012), http://dx.doi.org/10.1016/j.electacta.2012.11.057

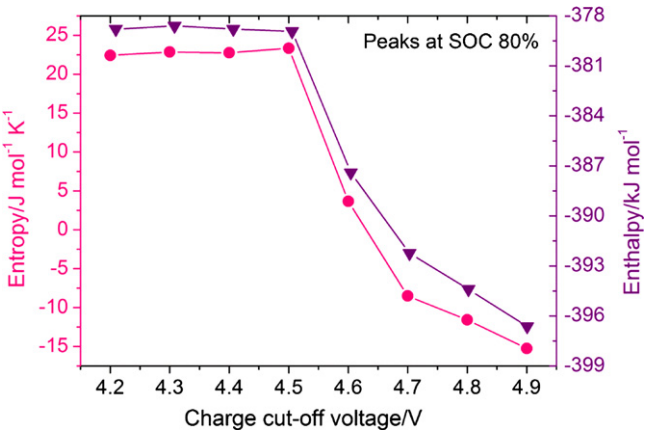

Fig. 9. Evolution of the entropy and enthalpy peaks intensity at 80% SOC with charge cut-off voltage.

the backscattering geometry at room temperature; excitation was carried out with the 514 nm radiation of an argon ion laser.

3. Results and discussion

3.1. Electrochemical cycling data

Fig. 1 shows the discharge profiles at step (iv) of COV2 test cells between 4.2 V and 2.75 V under C/4 rate (10 mA). Both the discharge voltage and the discharge capacity decreased as result of overcharging suggesting increased cells' polarization and electrodes structure degradation. Table 1 displays the charge and discharge test results including q_{C2}, q_{D3}, q_{D4} together with $\langle e_{C2} \rangle$ and $\langle e_{D4} \rangle$, the average charge and discharge voltages of steps (ii) and (iv), respectively. Table 1 also shows the discharge capacity loss (%) between step (i) and step (iv) for the COV2 tests cells.

The charge capacity q_{C2} increased dramatically between 4.2 V and 4.9 V COV. This denotes a partial delithiation of the LCO cathode and most likely some electrolyte oxidative decomposition. Similarly the discharge capacity q_{D3} increased with COV. Moreover, the cycle efficiency between q_{C2} and q_{D3} deceased significant to reach 88% at 4.9 V.

The discharge capacity loss q_{CL} showed in Table 1 also increased with COV to reach ~19% at 4.9 V. At 19% capacity loss, which correlates with the cell' end of life.

We have fitted the capacity loss q_{CL} vs. COV with an empirical polynomial function and found a 99.2% good fit with the following equation:

$$q_{CL}(\%) = 35.47 - 40.12(\mathrm{COV}) + 7.56(\mathrm{COV})^2 \quad (3)$$

Noteworthy is the ~100% increase in q_{CL} between 4.5 V and 4.6 V COV.

3.2. Thermodynamics studies

3.2.1. Open circuit voltage (OCV)

Fig. 2 shows the OCV profiles versus the charge capacity during step (iv). Differences in OCV values can be seen at the zero state of charge and for cells charged between 4.2 V and 4.6 V COV on one hand and for those charged between 4.7 V and 4.9 V on the other hand.

The initial OCV at zero state of charge increased with the COV. This suggests the presence of a partly de-lithiated cobalt oxide phase ($Li_{1-x}CoO_2$) in the cathode material, despite cells were discharged to 2.75 V. The rate of lithium deficiency 'x' probably increases with COV thus leading to higher initial OCV. Accordingly, even when aged cells are discharged to 2.75 V, there should be a residual delithiated phase in the cobalt oxide cathode and associated lithiated phase in the graphite anode. This conclusion will be later supported by ex situ XRD and Raman analyses.

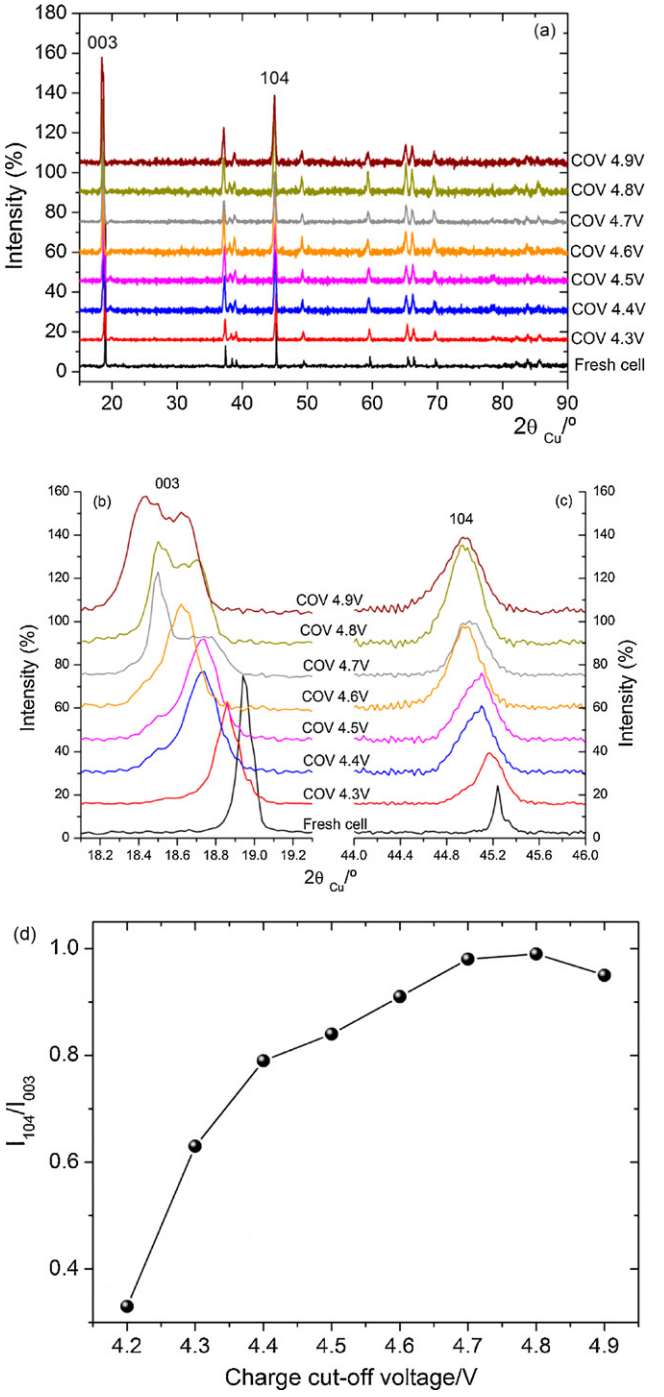

Fig. 10. X-ray diffraction patterns of $LiCoO_2$ before and after overcharge: (a) full pattern, (b) in the (0 0 3) peak area, (c) in the (1 0 4) peak area, and (d) evolution of the 1 0 4/0 0 3 peaks intensity ratio with COV.

The OCV traces in Fig. 2 splits in two sets; a first set where 4.2 V ≤ COV ≤ 4.6 V and a second set where 4.7 V ≤ COV ≤ 4.9 V, the later set exhibiting higher OCV values. This suggests a higher heterogeneous character of degraded cathodes for COV equal to or higher than 4.7 V, which correlates well with the striking decrease in the discharge capacity q_{D4} above 4.6 V COV as showed in Fig. 1 and in Table 1.

Please cite this article in press as: K. Maher, R. Yazami, Effect of overcharge on entropy and enthalpy of lithium-ion batteries, Electrochim. Acta (2012), http://dx.doi.org/10.1016/j.electacta.2012.11.057

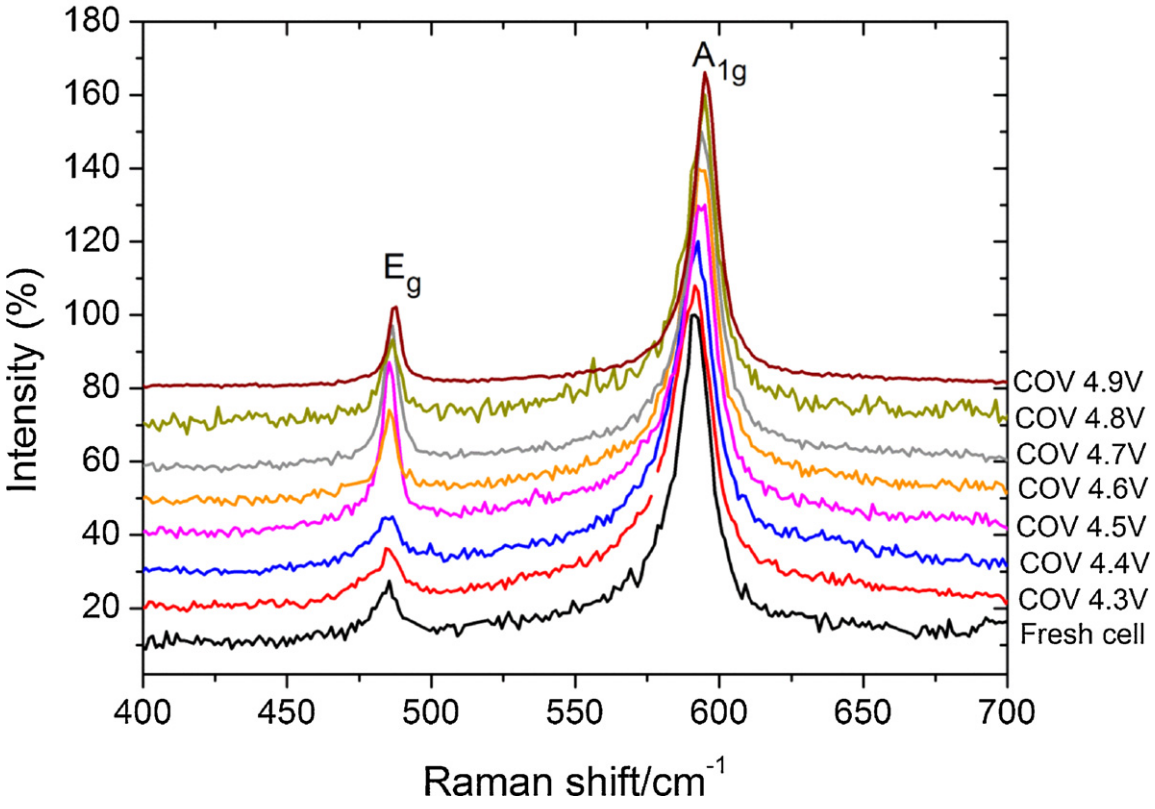

Fig. 11. Raman spectra of LCO cathodes at different COV.

3.2.2. Entropy and enthalpy profiles

3.2.2.1. Fresh cells. Typical entropy and enthalpy profiles of a cell cycled between 2.75 V and 4.2 V (fresh cells) are displayed in Figs. 3 and 4, respectively. The curves show changes in slope together with minima and maxima values. Those changes should be associated with onsets of electrode processes taking place at the anode and cathode materials, such phase transitions.

Using our previous thermodynamics data achieved in Li/Li_xC_6 (graphite) [1] and in Li/Li_xCoO_2 half-cells [4], we found that the entropy and enthalpy profiles shown in Figs. 3 and 4, respectively,

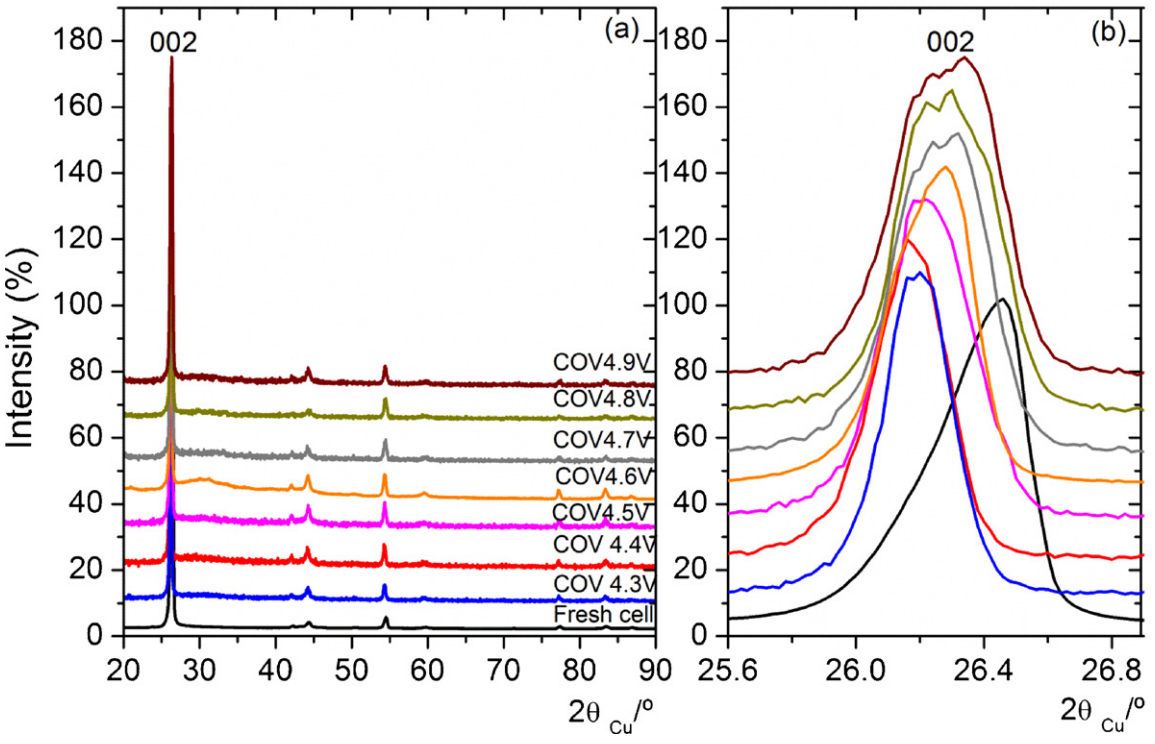

Fig. 12. X-ray diffraction patterns of the graphite anode before and after overcharge: (a) full pattern and (b) in the (0 0 2) peak area.

Please cite this article in press as: K. Maher, R. Yazami, Effect of overcharge on entropy and enthalpy of lithium-ion batteries, Electrochim. Acta (2012), http://dx.doi.org/10.1016/j.electacta.2012.11.057

fit well with a full cell consisting of the graphite anode and a lithiated cobalt oxide cathode. In fact, the entropy and enthalpy of a full cell result from the arithmetic difference between the corresponding states functions in the cathode and in the anode according to:

$$\Delta S(\text{full cell}) = \Delta S(\text{cathode}) - \Delta S(\text{anode}) \quad (4)$$

and

$$\Delta H(\text{full cell}) = \Delta H(\text{cathode}) - \Delta H(\text{anode}) \quad (5)$$

Therefore, any change in ΔS and ΔH profiles that takes place in the anode and the cathode should reflect in the ΔS and ΔH profile of the full cell. In the specific case of the graphite anode, changes in the ΔS and ΔH profiles go together with staging in Li_xC_6 [1], whereas as in the case of the lithiated cobalt oxide cathode, changes in thermodynamics data relate to a succession of phase transitions involving hexagonal phases and the monoclinic phase [4]. The onsets of phase transitions in the anode and the cathode are indicated in Figs. 3 and 4 by A_i and C_i letters, respectively. For instance, the stage 2 to stage 1 transition in graphite that takes place at $x = 0.5$ in Li_xC_6 corresponds to A_2 whereas the transition from hexagonal phase to a monoclinic phase that takes place at $Li_{0.55}CoO_2$ is marked C_4 in the figures.

One interesting aspect of accurate electrochemical thermodynamics measurements (ETMs) is that they allow the anode and the cathode chemistry of a full cell to be determined without a need to open it and analyse the electrode materials. ETM is a non-destructive analysis tool that applies in much more convenient way to reveal cells chemistry as compared with other heavier and more expensive high energy diffraction and spectrometry techniques such as those using X-ray, gamma and neutron radiations.

3.2.2.2. Aged cells.

3.2.2.2.1. COV1 vs. COV2 tests. In order to evaluate the effect of extended cells exposure to high voltage on the thermodynamics properties, we have drawn in Figs. 5 and 6 the entropy profiles of cells that have undergone COV1 and COV2 ageing protocols at COV of 4.6 V and 4.9 V, respectively. Fig. 5 (COV = 4.6 V) shows only a minor change in the entropy profile consisting particularly of a slight shift in the peak position around 80% SOC. On contrast, the curves in Fig. 6 (COV = 4.9 V) show a much pronounced shift towards lower SOC values for the COV2 cells. A larger shift in COV2 vs. COV1 entropy curves denotes stronger electrode material degradation when cells are exposed to higher voltages for longer durations.

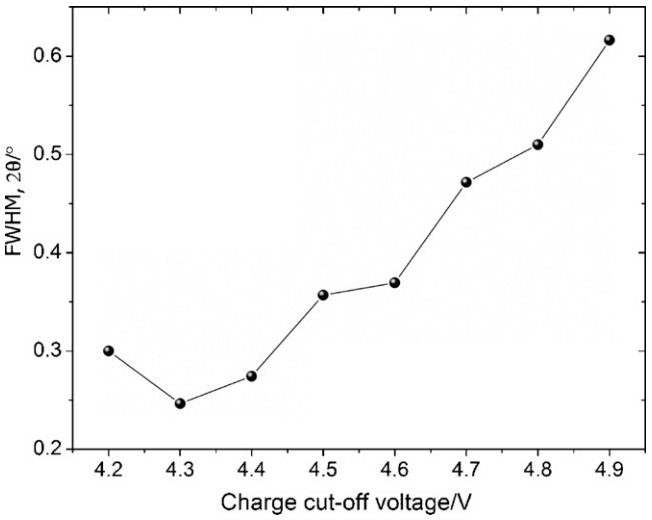

Fig. 13. Evolution of the graphite anode 002 peak full width at half-maximum (FWHM) vs. COV.

3.2.2.2.2. COV2 series. In this section we will show entropy and enthalpy results only for cells aged under the COV2 ageing protocol only. Figs. 7 and 8 compile the entropy and enthalpy profiles vs. SOC, respectively. Noticeable changes in the entropy and enthalpy profiles occur in the following SOC areas: 0%, ~5% and in ~60–90%, in particular at the C_2 peak around 80% SOC. Note the higher

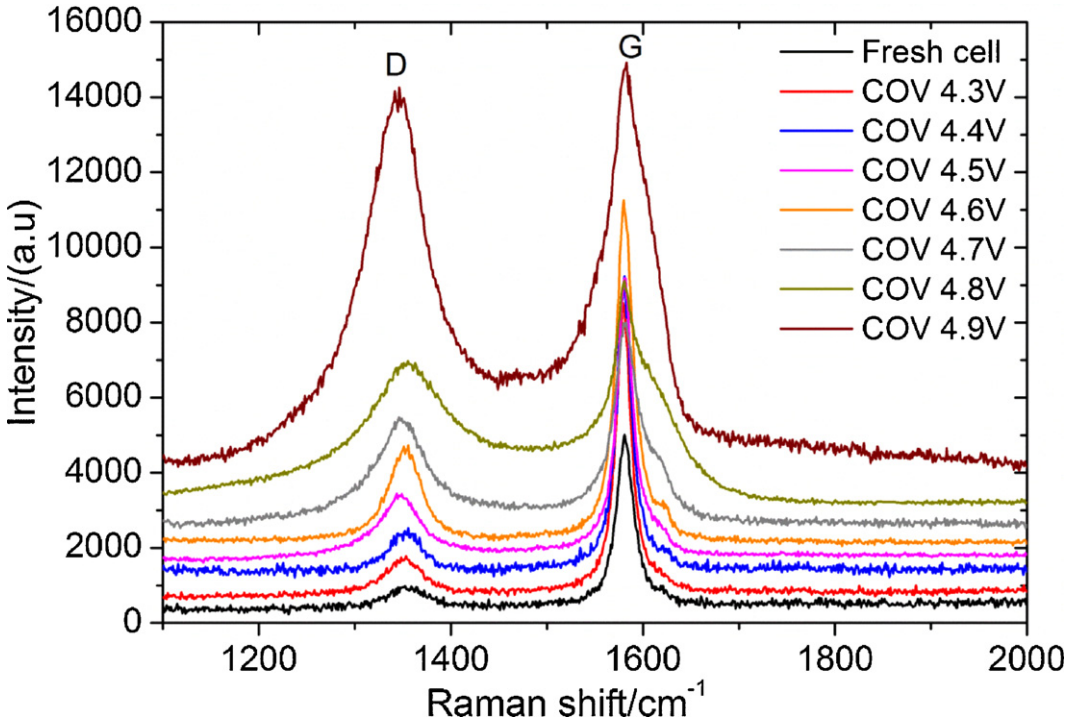

Fig. 14. Raman spectra of the graphite anode at different COV.

Please cite this article in press as: K. Maher, R. Yazami, Effect of overcharge on entropy and enthalpy of lithium-ion batteries, Electrochim. Acta (2012), http://dx.doi.org/10.1016/j.electacta.2012.11.057

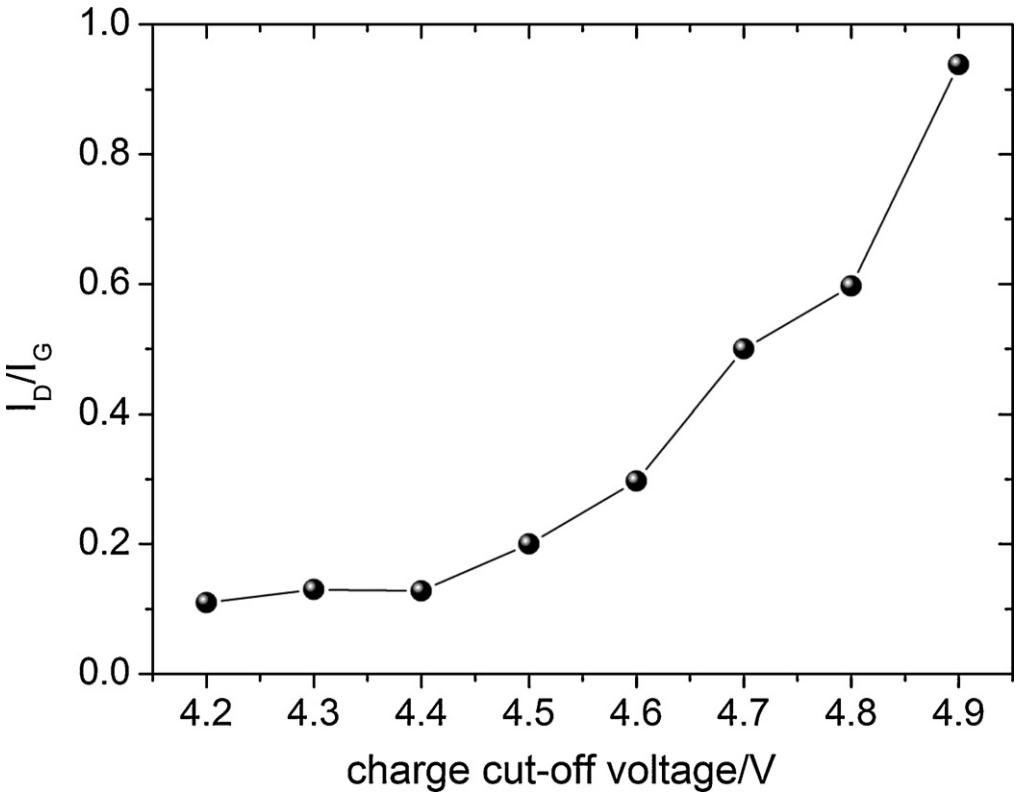

Fig. 15. Evolution of the I_D/I_G intensity ratio of the Raman D band and the G band of the graphite anode with COV.

resolution in the enthalpy profiles of Fig. 8 in the 40–70% SOC area as compared to the entropy ones of Fig. 7.

For the C_2 peak at 80% SOC the entropy and enthalpy peak intensity traces vs. COV are depicted in Fig. 9. In both entropy and enthalpy traces the peaks intensity remained almost unchanged up to COV of 4.5 V. The peaks intensity then rapidly decreased. This is consistent with the change in the OCV profiles of Fig. 2 and denotes a rapid degradation of the cathode material for COV above 4.5 V.

3.3. Post-mortem electrode materials analyses

X-ray powder diffraction and Raman spectroscopy were used to investigate the effect of high voltage charging under the COV2 protocol of the lithium cobalt oxide cathode and the graphite anode on crystal structure. The electrodes were taken from cells discharged to 2.75 V.

3.3.1. Lithium cobalt oxide (LCO) cathode

Fig. 10(a) shows the full XRD charts of LCO cathode materials at different COV. The diffraction angle areas where the 0 0 3 peak and the 1 0 4 peak appear are magnified in Fig. 10(b) and (c), respectively. The relatively narrow peaks at 18.9° and 45.25° of the "fresh cell" in Fig. 10(b) and (c) correspond to the 0 0 3 and the 1 0 4 peak of fully lithiated LCO, respectively. As the COV increases the 0 0 3 and the 1 0 4 peaks shifted towards lower angles in the 2θ peak angular position and became broader. Such a shift in the peak position results from residual lithium vacancies in $Li_{1-x}CoO_2$. In fact the c-parameter of the hexagonal phase increases as lithium is extracted from LCO for $0 < x < 0.5$ composition range in $Li_{1-x}CoO_2$ [8–10]. The other noticeable feature is the split of the 0 0 3 peak to two peaks for COV ≥ 4.7 V. This may relate to the formation of a disordered phase involving a Li and Co cation mixing [11,12]. Fig. 10(d) shows the COV dependence of the I_{104}/I_{003} peak intensity ratio [13]. The later ratio increases with COV, which suggests an increase in the rate of the Li and Co cation mixing with the cathode overcharge ageing.

Fig. 11 shows the Raman scattering (RS) profiles of LCO cathodes of different COV. Two Raman modes are observed, at 485 and at 595 cm^{-1}, and can be attributed to the E_g and A_{1g} modes, respectively, of the spectroscopic space group (D^5_{3d}) corresponding to $Li_{1-x}CoO_2$ of the layered rock-salt structure ($R\bar{3}m$ space group) [14]. However, there is no RS evidence of the formation of a pure spinel structure ($Fd3m$ space group), as the characteristic strongest peak 688 cm^{-1} corresponding to the F_{2g} mode is absent from the spectra. Accordingly, although cation mixing increased significantly with COV, a pure spinel phase did not form.

3.3.2. Graphite anode

The XRD charts of the graphite anode at different COV are depicted in Fig. 12(a) (full spectra) and Fig. 12(b) (the 0 0 2 peak area). Compared to the initial fresh cell, the 0 0 2 peak position shifted to lower diffraction angles and the peak broadened with increased COV. A shift to lower angles results of larger graphene interlayers spacing coming from residual intercalated lithium in the graphite structure. The 0 0 2 peak broadening as depicted in Fig. 13 should result from increased graphene layers stacking disorder. It is interesting to note that the 0 0 2 peak position in the "fresh cell" falls at $2\theta = 26.48°$, which corresponds to an interlayer spacing $d_{002} = 3.365$ Å is slightly higher than $d_{002} = 3.350$ Å of high crystalline graphite. Accordingly, the graphite used in our test cells should still contain some residual turbostratic disorder.

The XRD results are consistent with the Raman Scattering ones displayed in Fig. 14. The two active modes at 1350 cm^{-1} (D-mode) and 1590 cm^{-1} (G-mode) are typical of graphite materials with more or less amounts of crystal structure disorder [15–17]. The presence of a weak D-mode peak in the anode material taken from a fresh cell is consistent with XRD results discussed above.

Please cite this article in press as: K. Maher, R. Yazami, Effect of overcharge on entropy and enthalpy of lithium-ion batteries, Electrochim. Acta (2012), http://dx.doi.org/10.1016/j.electacta.2012.11.057

The Raman active modes intensity ratio I_D/I_G depicted in Fig. 15 increases with COV indicating an increase in the graphene layers disorder upon high voltage ageing.

Differential (or incremental) capacity methods ($\partial Q/\partial E = f(E)$) developed by Ohzuku et al. [18] have been widely used in the characterization of electrode processes in both half cells [18–20] and full cells [21]. Typically, $\partial Q/\partial E$ curves derive from slow rate charge and discharge profiles or OCV profiles with peak(s) appearing at voltages E of thermodynamics significance, mostly related to free energy. By adding the temperature parameter in our study we are able to break the free energy in its two components; the enthalpy and the entropy and get further insights on the electrode thermodynamics, which isotherm studies do not allow to achieve.

4. Conclusion

Thermodynamics study on aged lithium-ion cells at their charge state revealed drastic changes in the entropy and the enthalpy profiles. We found particular state of charge domains where changes in thermodynamics properties are more pronounced; in particular at zero SOC and around 80% SOC. We also found a steep increase in capacity loss between 4.5 V and 4.6 V COV indicating accelerated electrode and/or electrolyte degradation in the 4.5–4.6 V COV range. Changes in thermodynamics properties were tentatively related to crystal structure deterioration at the anode (0% SOC) and the cathode (80% SOC), which we confirmed by ex situ XRD and Raman scattering analyses. On the graphite anode side we found a shift in the 0 0 2 XRD peak towards lower angles indicating residual intercalated lithium in the graphite structure together with peak broadening resulting from graphene layers stacking disorder, a result confirmed by RS. On the LCO side, we also found a shift towards lower angles of the 0 0 3 diffraction peak suggesting a sizeable amount of lithium vacancies in LCO and also peak broadening and splitting as COV increased. The occurrence of lithiated graphite and delithiated LCO in the cells discharge state accounts for the higher observed OCV at “zero” SOC. In fact the cells at their theoretical full discharge state are still partly charged although, as a paradox that charge is not available.

Acknowledgement

The authors would like to thank Mrs. Yin Ting Teng for her help in the Raman experiments.

References

[1] Y. Reynier, R. Yazami, B. Fultz, The entropy and enthalpy of lithium intercalation into graphite, Journal of Power Sources 850 (2003) 119.
[2] Y. Reynier, R. Yazami, B. Fultz, Thermodynamics of lithium intercalation into graphites and disordered carbons, Journal of the Electrochemical Society 151 (2004) A422.
[3] Y. Reynier, R. Yazami, B. Fultz, I. Barsukov, Evolution of lithiation thermodynamics with the graphitization of carbons, Journal of Power Sources 165 (2007) 552.
[4] Y. Reynier, J. Graetz, T. Swan-Wood, P. Rez, R. Yazami, B. Fultz, The entropy of Li intercalation in Li_xCoO_2, Physical Review B 70 (2004) 174304.
[5] R. Yazami, Thermodynamics of Electrode Materials for Lithium-Ion Batteries, in: K. Ozawa (Ed.), Chapter 5 in Lithium Ion Rechargeable Batteries, Materials, Technology and New Applications, Wiley-VCH, Weinheim, 2009, p. 67.
[6] R. Yazami, Y. Ozawa, H. Gabrisch, B. Fultz, Mechanism of electrochemical performance decay in $LiCoO_2$ aged at high voltage, Electrochimica Acta 50 (2004) 385.
[7] S.S. Choi, H.S. Lim, Factors that affect cycle-life and possible degradation mechanisms of a Li-ion cell based on $LiCoO_2$, Journal of Power Sources 111 (2002) 130.
[8] T. Ohzuku, A. Ueda, Factors that affect cycle-life and possible degradation mechanisms of a Li-ion cell based on $LiCoO_2$, Journal of the Electrochemical Society 141 (1994) 2972.
[9] G.G. Amatucci, J.M. Tarascon, L.C. Klein, CoO_2, the end member of the Li_xCoO_2 solid solution, Journal of the Electrochemical Society 143 (1996) 1114.
[10] Z. Chen, Z. Lu, J.R. Dahn, Staging phase transitions in Li_xCoO_2, Journal of the Electrochemical Society 149 (2002) A1604.
[11] Y. Ozawa, R. Yazami, B. Fultz, Study of self-discharge of $LiCoO_2$ cathode materials, Journal of Power Sources 119 (2003) 918.
[12] H. Gabrisch, R. Yazami, B. Fultz, Hexagonal to cubic spinel transformation in lithiated cobalt oxide: TEM investigation, Journal of the Electrochemical Society 151 (2004) A891.
[13] M. Yoshio, H. Tanaka, K. Tominaga, H. Noguchi, Synthesis of $LiCoO_2$ from cobalt organic-acid complexes and its electrode behavior in a lithium secondary battery, Journal of Power Sources 40 (1992) 347.
[14] M. Inaba, Y. Todzuka, H. Yoshida, Y. Grincourt, A. Tasaka, Y. Tomida, Z. Ogumi, Raman-spectra of $LiCo_{1-y}Ni_yO_2$, Chemistry Letters 10 (1995) 889.
[15] F. Tuinstra, J.L. Koenig, Raman spectrum of graphite, Journal of Chemical Physics 53 (1970) 1126.
[16] K. Nakamura, M. Fujitsuka, M. Kitajima, Disorder-induced line broadening in 1st-order Raman-scattering from graphite, Physical Review B 41 (1990) 12260.
[17] M. Inaba, H. Yoshida, Z. Ogumi, T. Abe, Y. Mizutani, M. Asano, In-situ Raman-study on electrochemical Li-intercalation into graphite, Journal of the Electrochemical Society 142 (1995) 20.
[18] T. Ozhuku, M. Kitagawa, T. Hirai, Electrochemistry of manganese-dioxide in lithium non aqueous cell: X-ray diffractional study on the reduction of spinel-related manganese-dioxide, Journal of the Electrochemical Society 137 (1990) 769.
[19] K. West, B. Zachau-Chritiansen, S.V. Skaarup, F.W. Paulsen, Lithium insertion in sputtered vanadium-oxide film, Solid State Ionics 57 (1992) 41.
[20] K. West, B. Zachau-Chritiansen, T. Jacobsen, S.V. Skaarup, Vanadium-oxide xerogels as electrodes for lithium batteries, Electrochimica Acta 38 (1993) 1215.
[21] M. Dubarry, B.Y. Liau, M.-S. Chen, S.-S. Chyan, K.-C. Han, W.-T. Sie, S.-H. Wu, Identifying battery aging mechanisms in large format Li ion cells, Journal of Power Sources 196 (2011) 3420.

Please cite this article in press as: K. Maher, R. Yazami, Effect of overcharge on entropy and enthalpy of lithium-ion batteries, Electrochim. Acta (2012), http://dx.doi.org/10.1016/j.electacta.2012.11.057